Intracellular Fluorescent Probe Concentrations by Confocal Microscopy

Charles Fink, Frank Morgan, and Leslie M. Loew

Department of Physiology and Center for Biomedical Imaging Technology, University of Connecticut Health Center, Farmington, Connecticut 06030 USA

ABSTRACT   A general method is described that takes advantage of the optical sectioning properties of a confocal microscope to enable measurement of both absolute and relative concentrations of fluorescent molecules inside cells. For compartments within cells that are substantially larger than the point spread function, the fluorescence intensity is simply proportional to the concentration of the fluorophore. For small compartments, the fluorescence intensity is diluted by contributions from regions outside the compartment. Corrections for this dilution can be estimated via calibrations that are based on the intensity distribution found in a computationally synthesized model for a cell or organelle that has been blurred by convolution with the microscope point spread function. The method is illustrated with four test cases: estimation of intracellular concentration of a fluorescent calcium indicator; estimation of the relative distribution between the neurite and soma of a neuronal cell of the InsP$_3$ receptor on the endoplasmic reticulum; estimation of the distribution of the bradykinin receptor along the surface of a neuronal cell; and relative distribution of a potentiometric dye between the mitochondria and cytosol as a means of assaying mitochondrial membrane potential.

INTRODUCTION

Fluorescence measurements with a spectrofluorometer offer a simple, linear, sensitive method for determining the concentrations of fluorescent analytes. The use of a fluorescence microscope to achieve the same end within a cell is more problematic (Wang and Taylor, 1989a,b). A fundamental difference between the two measurements accounts for the difficulty encountered in microscopy. The spectrofluorometer employs cuvettes with fixed shapes and dimensions for the fluorescent solution. Therefore, the volume of dye solution that is sampled by the optics is constant from experiment to experiment, and only the concentration of dye can affect the fluorescence intensity. Different cells present variably sized "cuvettes" to the optics of a fluorescence microscope, so that an intensity depends on both dye concentration and the effective size of the sampled volume. For experiments that aim to measure nonuniform dye distributions within single cells by quantitative digital imaging, the variable thickness of different regions of a cell can severely impede interpretation of the measured intensities.

An effective approach to this problem has been the use of dual-wavelength ratio imaging microscopy (Tsien and Poenie, 1986; Bright et al., 1987). This method is especially useful for fluorescent ion indicator dyes with spectra that undergo wavelength shifts as a function of ion concentration. Because the dye concentration and cell thickness will affect the intensity proportionately at both wavelengths, whereas ion concentration affects the respective intensities differentially, the ratio is dependent solely on the ion concentration. In this way, a map of ion concentration throughout a two-dimensional image of a cell can be developed.

When the distribution of a fluorescently labeled molecule is of interest, a variant of the dual-wavelength ratio method is to use a second reference fluorophore with different spectral properties that is known to have a uniform intracellular distribution (Debiaso et al., 1987, 1988). The ratio of images acquired at the respective wavelengths should normalize away any errors due to variations in thickness. In practice, it is difficult to be sure that a given reference dye is, in fact, evenly distributed. Differences in the rates of dye leakage and photobleaching can also lead to errors when kinetic processes are the subject of sequences of such dual-wavelength images.

The confocal microscope can obviate the problem of measuring dye concentrations within cells, because the optics have the effect of creating a phantom cuvette that is thinner than the thickness of the cell. As long as the optical slice is centered within the cell and is totally encompassed by the cellular volume, the intensity measured at each voxel by the confocal microscope should be proportional to the dye concentration. This laboratory has developed a method for measuring membrane potential based on this principle (Farkas et al., 1989; Loew, 1993, 1998). The idea is to allow a fluorescent membrane permeant cation to equilibrate across the cell membrane. At equilibrium, the dye distribution is governed by the Nernst equation, so that the ratio of dye concentration between the cytosol and the extracellular volume can be used to calculate the membrane potential. Despite the large difference in the volume of these two spaces, the volume probed by the confocal microscope is smaller than either. Therefore, the ratio of fluorescence intensities from these two compartments is equal to the ratio of concentrations.

A variation of this approach was the subject of a fruitful collaboration between this laboratory and Fred Fay, Walter

Carrington, and Richard Tuft of the Biomedical Imaging Group at the University of Massachusetts Medical School. The aim was to extend the measurement of membrane potential with Nernstian dyes to the mitochondrial membrane. Because mitochondria are generally below the resolution limit of a confocal microscope, the simple measurements described above will not suffice. Our strategy (Loew et al., 1993) was to use a wide-field microscope to image a series of planes through the thickness of a cell exposed to the dye. This 3D image was subjected to the deconvolution algorithm developed by Carrington et al. (Carrington and Fogarty, 1987; Fay et al., 1989; Carrington, 1990; Carrington et al., 1990) to restore the out-of-focus light to its proper point of origin. However, the axial resolution of even the best microscope optics is never better than ∼500 nm − above the diameter of typical mitochondria. So an additional procedure was developed to assess the error inherent in the measurement and thereby enable a calibration of the ratio of fluorescence between the mitochondria and the cytosol. The method used a 3D computer model of a mitochondrion based on dimensions derived from electron micrographs. The model was first blurred with the point spread function of the microscope and then subjected to the restoration algorithm. The intensity in the resulting image was compared to the intensity of the original model to generate the appropriate correction factor.

In this paper we employ the same blurring procedure to assess the accuracy of relative dye concentrations in confocal micrographs instead of restored 3D wide-field images. We use the method to measure mitochondrial membrane potential from the calibrated ratio of a Nernstian dye in NIH 3T3 fibroblasts. The general approach is also extended to examinations of cellular distributions of dye for three common situations:

1. Determination of the absolute concentration of a fluorescent calcium indicator.

2. Determination of the distribution of a fluorescently labeled antigen within the endoplasmic reticulum of a neuronal cell.

3. Determination of the distribution of a plasma membrane antigen along the surface of a neuronal cell.

For all of these cases, we employ differentiated N1E-115 neuroblastoma cells because their complex morphology presents a good test bed for the development of these approaches.

MATERIALS AND METHODS

Cell culture

N1E-115 neuroblastoma cells (obtained from Dr. M. Niremberg, National Institutes of Health) were grown and maintained in Dulbecco's modified Eagle's medium (DMEM) containing 10% fetal bovine serum and 1% antimitotics/antimycotics, and kept in a 5% CO_2 incubator at 37°C. Cells were grown until 50% confluent before plating on individual coverslips. Differentiation was induced by decreasing the serum level to 0.5% fetal bovine serum and introducing 1% dimethylsulfoxide; differentiation to the neronal morphology was complete after 60–72 h. For microscopy, coverslips were transferred to an open-welled plastic chamber and kept in

Earle's balanced salt solution (EBSS) buffered to pH 7.4 with 10 mM HEPES.

Mouse NIH 3T3 fibroblast cells (obtained from the American Type Culture Collection) were grown and maintained in DMEM containing 10% calf serum (CS) and switched to low-serum medium (0.5% CS) for 48 h before microscopy. Cells were kept in a 5% CO_2 incubator at 37°C and plated on coverslips, which were transferred to an open-welled plastic chamber and kept in buffered EBSS for viewing on the inverted Zeiss (Thornwood, NY) LSM410 confocal microscope.

Immunolocalization

Differentiated N1E-115 neuroblastoma cells were fixed by a 10-min incubation at room temperature in a 4% paraformaldehyde/0.1% glutaraldehyde solution. After washing with phosphate-buffered saline (PBS), fixed cells were then permeabilized in 0.01–0.1% Triton-X/PBS solution for 2–5 min at room temperature, followed by 2 h of nonspecific blocking in a 5% milk/PBS solution. After washing, the cells were incubated with the primary antibody (in a 3% bovine serum albumin (BSA)/PBS solution) for up to 19 h at 4°C. Primary antibodies used were rabbit anti-BK2-receptor (1/50 dilution; generously donated by Werner Esterl-Muller) and rabbit anti-InsP$_3$-receptor-I (1/100; a generous donation from Barbara Ehrlich). For the negative controls, either the primary antibody was omitted or the primary was substituted with IgG of the appropriate animal. After the wash, the cells were incubated with the secondary antibody (anti-rabbit rhodamine, 1/100 dilution; Molecular Probes) in 3% BSA/PBS for 1 h at room temperature. After a final wash, the coverslips were mounted on glass slides in a glycerol/PBS anti-fade solution (SlowFade, Molecular Probes) and sealed with nail polish. Cells were then visualized with the confocal microscope, using a 568-nm excitation laser line, with emission collected through a 630-nm high-pass emission filter. Three-dimensional section analysis was carried out with a VoxelView (Vital Images, Minneapolis, MN) software package on Silicon Graphics (Mountain View, CA) workstations.

Fura-2 imaging

Differentiated N1E-115 neuroblastoma cells were treated with 5 μM fura-2/AM (Molecular Probes) and 0.025% Pluronic-F127 for 30–60 min at room temperature, followed by a 30-min recovery in EBSS at 37°C. Cells were then visualized with the confocal microscope, using a 364-nm excitation laser line, with emission collected from 515–560 nm. Before visualizing, cells were exposed to 10 μM ionomycin and allowed to equilibrate to saturating calcium levels for 2 min. Calibration slides were made by preparing various concentrations of fura-2 salt in EBSS, and imaging the dye between two coverslips with the same parameters as used for the cellular fura-2 imaging.

TMRE imaging

Tetramethyl rhodamine ethyl ester (TMRE) was synthesized in our laboratory (Ehrenberg et al., 1988), but may also be obtained from Molecular Probes (Eugene, OR). Coverslips with NIH 3T3 fibroblasts were mounted on a thermostatted perfusion chamber at 37°C and equilibrated with 100 nM TMRE for 10 min before microscopy. The fluorescence was excited with the 568-nm laser line and collected through a 595-nm long-pass filter.

Point spread function generation

Rhodamine and UV fluorescent microspheres (100 nm; Molecular Probes) were diluted appropriately and allowed to settle onto coverslips. Slides were imaged on the confocal microscope, focusing on the region of interest containing an isolated bead. Point spread functions (PSFs) were obtained with the same optics, filters, zoom settings, and pinhole aperture as the respective parameters for the fura-2, anti-InsP$_3$-receptor, and anti-BK2-

receptor experiments. In the case of the mitochondria images, the fluorescent microspheres were added to the coverslips containing the NIH 3T3 cells and were imaged before equilibration of the cells with TMRE. A through-focus series with 100-nm steps was taken with sufficient width so that all emitted fluorescence from the bead was captured. Background intensity levels were carefully determined and subtracted from the data; any pixels outside the biconical solid volume of the PSF with residual background could be then eliminated by a simple thresholding operation.

Model creation

The models are created on a Silicon Graphics O2 workstation (Mountain View, CA) with the freely available ray-tracing program POV-Ray(2.2), using the simple geometric primitives and constructive solid geometry contained within the program. The soma is created as a hemisphere, the neurite is a split cylinder, and the growth cone is a disc with the same thickness as the neurite; the diameters of these objects approximate the respective width, in pixels, of the corresponding features of the cell in the image to be analyzed. For the mitochondrial model, a cylinder with a length of 1 μm perpendicular to the optical axis and a diameter of 350 nm was employed (see Results). The model is rasterized by positioning a viewpoint parallel to the z axis over the center of the model and intersecting the model with a plane parallel to the xy axis at a fixed distance from the viewpoint. Each plane in the z axis is sampled by translating the model parallel to the z axis through the fixed plane. The intensity of the voxels in the model is uniformly set to 100 units. The resolution of the model is initially set to 4 times the pixel resolution of the image and its corresponding PSF to supersample the geometry; it is then binned down to the final pixel resolution providing appropriately interpolated edges.

Convolution of PSF with the model

The convolution of the volume model data with the experimental PSF was performed with a simple C program. Each point in the convolution result is the product of the normalized 3D PSF and the corresponding 3D subvolume centered around that point in the volume data. The model data are padded with zero values around all edges (x, y, z) to visualize the effect of the PSF on "out-of-focus" data points.

RESULTS

Characterizing a confocal microscope by convolving a model image with a point spread function

Because the optical microscope is an approximately linear device, the way it blurs out a complex object is simply a linear combination of the way it blurs out each point in the object. The left column of Fig. 1 displays two orthogonal slices through a typical point spread function (PSF), the blurred image of a subresolution fluorescent bead, from a high numerical aperture lens and a moderately narrow confocal aperture. Although this PSF is much tighter than that from a widefield microscope, it is important to examine its shape, so as to appreciate the limitations of the confocal optics for measuring dye concentrations in cells. In the plane perpendicular to the optical axis, the half-width of the PSF is 650 nm; in the axial direction the PSF has a half-width of 1.85 μm. These dimensions approximately describe the minimum size of a fluorescent object from which the center can yield an accurate intensity. This idea is illustrated with a series of rectangular solids in the middle

column of Fig. 1 and the corresponding blurred images in the right column resulting from convolutions with the PSF. The convolution is simply a linear combination of the PSF scaled to the intensity of the object at each point within the object. The images in the right-hand column represent the distortion of the true fluorescence distribution that would be imposed by the microscope optics that produced the PSF. As can be seen, the solid that is much smaller than the PSF is severely blurred. The intermediately sized rectangular solid has dimensions that are comparable to those of the PSF and has a maximum intensity that is reduced by $\sim$50% by the convolution. The largest solid retains its original fluorescence intensity through most of its volume; this validates the idea that the fluorescence intensity from the center of a large object is directly proportional to the concentration of the fluorophore.

Intracellular concentrations of fura-2

The calcium indicator fura-2 (Grynkiewicz et al., 1985) is frequently loaded into cells by methods that do not allow precise control of its intracellular concentration. This parameter is important because high levels of fura-2, or any ion indicator, can behave as a calcium buffer that will perturb the dynamics that it is there to probe. It may also be useful to have a precise method for measuring the fura-2 concentration to deliberately control the calcium buffer levels inside a cell. Application of confocal microscopy to measure the intracellular concentration of fura-2 in a neuronal cell is illustrated in Fig. 2.

A 3D image of a neuronal cell loaded with fura-2 was acquired; several optical sections are displayed in Fig. 2 *a*. The loading conditions were fairly typical: 5 μM fura-2AM with 0.025% Pluronic-F127 for 60 min at 22°C, followed by 30 min in dye-free solution at 37°C. These images were taken in the presence of 10 μm ionomycin, a calcium ionophore, so that the intracellular compartment was equilibrated to the same calcium concentration as the extracellular medium; although the wavelength for excitation, 364 nm, is close to the isosbestic point for the free versus calcium-bound forms of fura-2, the use of ionomycin ensured a valid comparison with the calibration from dye slides containing high Ca^{2+} concentrations (Fig. 2 *c*). Because the soma is significantly thicker than the axial extent of the PSF, the intensity measured in the center of the soma should not have suffered any blurring effect and should be amenable to direct calibration. This can be confirmed by using the PSF to convolve an approximate model of the cell, as shown in Fig. 2 *b*. As can be seen, the original intensity in the center of the soma is hardly affected by the blurring effect of the microscope, whereas the intensity in the neurite is reduced to $\sim$30%. Indeed, the maximum intensity in the neurite of Fig. 2 *a* is 30% of the intensity in the central planes through the soma, suggesting that throughout this cell the fura-2 distribution is generally quite even.

With the confocal microscope, a calibration of intensity against fura-2 concentration can be generated from a series
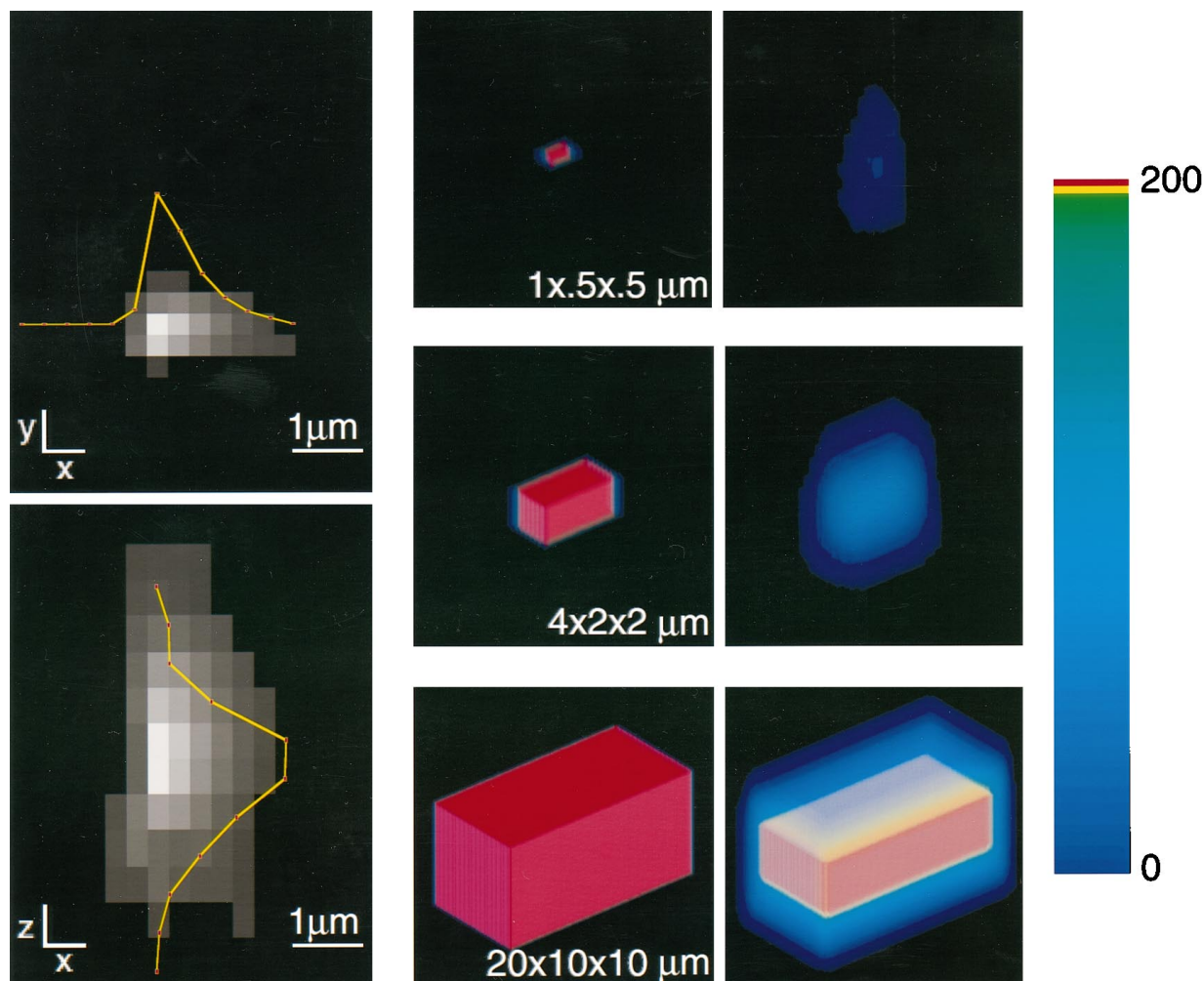
FIGURE 1 Model rectangular solids calibrate the limits of accurate intensity measurements with a confocal microscope. The left column shows slices through *xy* and *xz* planes of the PSF, corresponding to a 60× NA 1.4 Olympus objective and a confocal aperture setting of 30 on the Zeiss LSM410. The pixel resolution is 300 nm × 300 nm × 500 nm in *x*, *y*, and *z*, respectively. Line scans along the *x* and *z* axes are superimposed on the images to provide an indication of the shape of the intensity distribution in the PSF. The central column displays three computationally synthesized rectangular solids with uniform intensities of 200 units. The right column shows the results of the convolution of each solid with the PSF. The range of colors in the image is stretched to permit ready identification of regions of maximum intensity, as indicated by the color bar.

of reference solutions. In Fig. 2 *c*, the linearity of the intensity measured in a series of such solutions with the confocal microscope is demonstrated, using the same gain, black level, pinhole setting, and objective as in Fig. 2 *a*. A chamber formed from a rectangular hole in a plexiglass slide with a coverslip floor was placed on an inverted confocal microscope for these measurements. A fiduciary mark made with a black pen on the upper surface of the coverslip ensured that the focal plane was set 5 μm into the fura-2 solution, approximating the focal plane in the center of an adherent cell. Using this calibration line, we were able to measure the fura-2 concentration in a large number of cells. A histogram of the distribution of fura-2 concentrations from 123 cells is shown in Fig. 2 *d*. Interestingly, there was significant variability in the concentration of fura-2, even on the same coverslip. The average concentration was 38 μM $\pm$ 17 μM (mean $\pm$ SD; 123 cells). This variability could arise from the different surface-to-volume ratios in

these cells—a larger surface area permitting greater access for fura-2/AM to permeate the plasma membrane. It is also possible that the degree of differentiation could result in variable esterase levels within these cells. No attempt was made to correlate the data against either of these factors or other factors that might explain the variability. However, it should be noted that variable levels of fura-2 will result in variable levels of $[Ca^{2+}]_{cyt}$ buffering, which could affect the results of experiments using this popular indicator.

Estimation of the distribution of an intracellular fluorescent label

Confocal microscopy is most frequently used to study the spatial distribution or localization of a macromolecule within a cell. For questions related to the localization of a molecule to a particular subcellular structure or organelle,
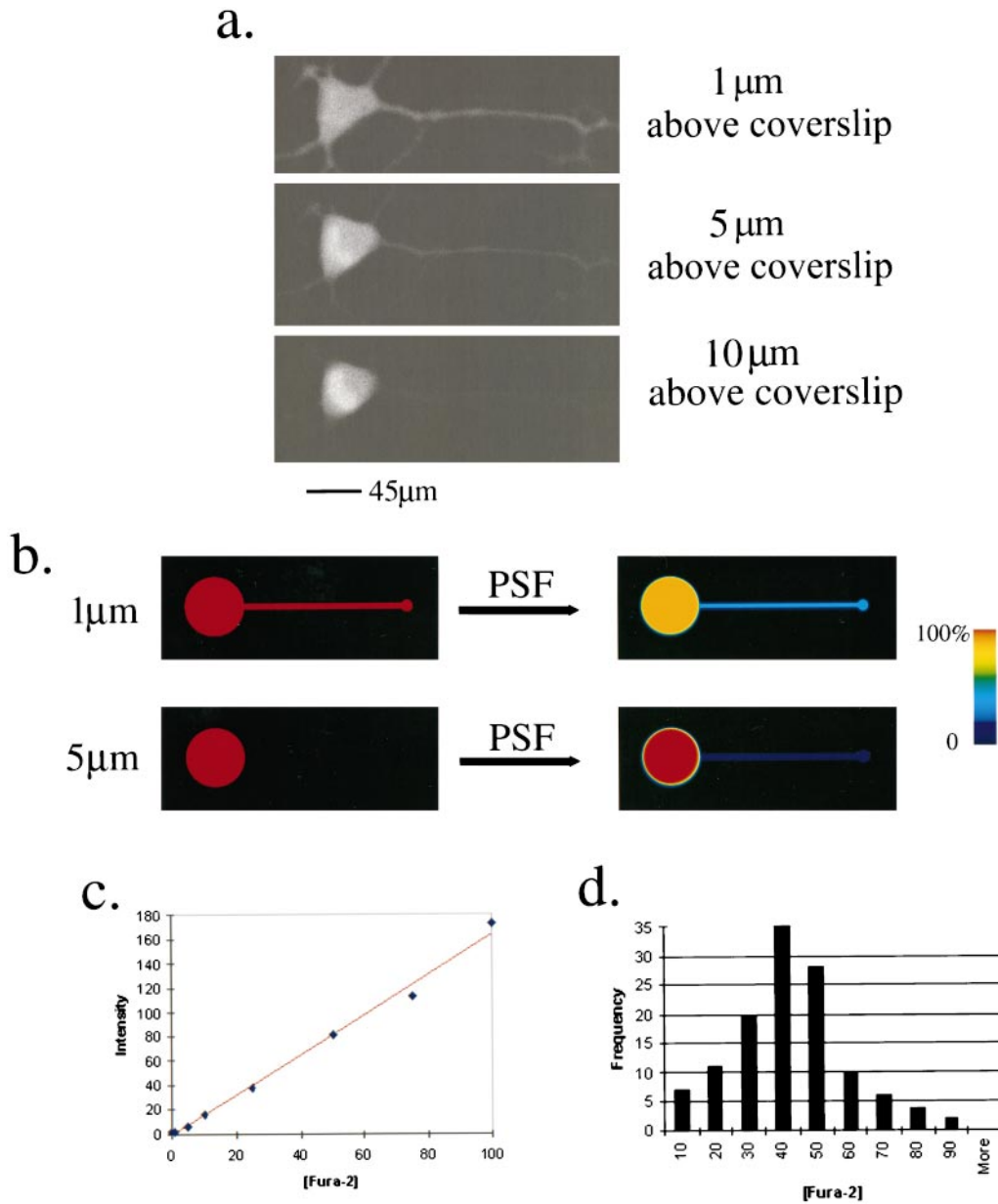
FIGURE 2 Estimation of fura-2 concentrations in single living cells. (*a*) N1E-115 neuroblastoma cells were loaded with fura-2 and imaged in *z*-series on the confocal microscope with a Zeiss 40× NA1.2 water immersion planapochromat objective with excitation at 364 nm and emission between 515 nm and 560 nm. Before imaging the cells were exposed to 10 μm ionomycin to equilibrate calcium levels with the media. Contrast and brightness settings were adjusted so that the intensity of the cell was below saturation and the background was close to zero. A *z*-series was taken through the cell at 1-μm intervals. Sections of this *z*-series are shown at 1, 5, and 10 μm above the coverslip. (*b*) A model of the cell in *a* was constructed from a hemisphere (representing the soma), a half-cylinder (representing the neurite), and a disc (representing the growth cone). The dimensions were assigned to approximate the corresponding portions of the cell as determined within the *xy* plane, where the resolution was best. The solid model was convolved with a PSF obtained from a subresolution bead under the same optical conditions as those used for the images in *a*. (*c*) Solutions of various fura-2 salt concentrations were imaged in a thin layer above a coverslip on the confocal microscope, with the microscope settings that had been used for imaging cells loaded with fura-2. A single scan was performed at a depth well within the solution, which showed no change in intensity over at least a 5-μm focal range; an average intensity was then measured in the center of the scanned field. This intensity is plotted against the concentration of fura-2 in the solution. A straight line with a slope of 0.6 intensity units/nM, $R = 0.99708$, was fit to this plot. (*d*) Many cells were imaged with the same parameters as previously used to determine the distribution of fura-2 concentration in N1E-115 neuroblastomas. A slice taken through the cells in which the intensity did not vary within ± 1 μm. The resulting intensity was converted to fura-2 concentration by the calibration developed in *c*. These fura-2 concentrations are displayed in a histogram for 123 cells.

the most common approach is to employ double immuno-fluorescence labeling. Using fluorescently labeled antibodies with different spectral characteristics, the colocalization of the unknown antigen with an antigen that is known to be associated with the organelle can be assessed directly within the same cell. In cases where the appropriate reference

antibody is unavailable, where it is desired to determine the distribution of a fluorescent label in a living cell, or where the distribution of the subcellular structure is itself not uniform and not resolvable, the use of a model convolved with a PSF can guide the direct interpretation of the confocal fluorescence image.

This is illustrated for the distribution of the endoplasmic reticulum (ER) in the differentiated N1E-115 cells. The variable thicknesses of these cells make it difficult to ascribe regional intensity variations to differences in the density of the ER as opposed to artifacts due to differences in the diameter of the neurite and soma. Fig. 3 *a* displays a volume-rendered image of a cell labeled with an antibody to the inositol trisphosphate receptor (type I)—an ER associated protein. As revealed especially in the *xz* sections, there is a lower fluorescence intensity in the neurite compared to the soma. Whether this truly reflects a difference in the density of ER can be assessed from the convolution of a 3D model containing a uniform intracellular density of fluorescent source molecules with an experimental PSF obtained under the same conditions as the image in Fig. 3 *a*. This is illustrated in Fig. 3 *b* for a model cell with the approximate dimensions of the cell in Fig. 3 *a*. The model could be improved by using a semiellipsoid rather than a hemisphere to model the soma; the ER-free region that corresponds to

the nucleus is also not modeled. Still, the soma is large enough that these details should not affect our ability to estimate differences in fluorophore densities relative to the neurite. The fluorescence in the neurite of the convolved model is diluted to $\sim\frac{2}{3}$ of that obtained in the center of the soma. However, in Fig. 3 *a*, the intensity in the neurite is $\sim$50% of that from the thickest part of the soma. Therefore, the results in Fig. 3 *a* indicate that either the ER density or the InsP$_3$ receptor density in the neurite is lower than in the soma. That the ER density is generally significantly lowered in the neurite has been confirmed by analysis of electron micrographs of these cells (data not shown).

Distribution of cell surface molecules

Plasma membrane receptors can be unevenly distributed along the surface of a cell to permit localized or directed responses to a stimulus. For a cell with a complex shape in which the intensity from different regions of the fluorescently labeled membrane may overlap, interpretation of images of cell surface molecules can benefit from the evaluation of blurred models. Because the membrane of a cell is $\sim$50 Å in thickness, it is clearly below the resolution limit of the confocal microscope, but it can be modeled as a one-voxel shell completely enclosing the volume of the cell.
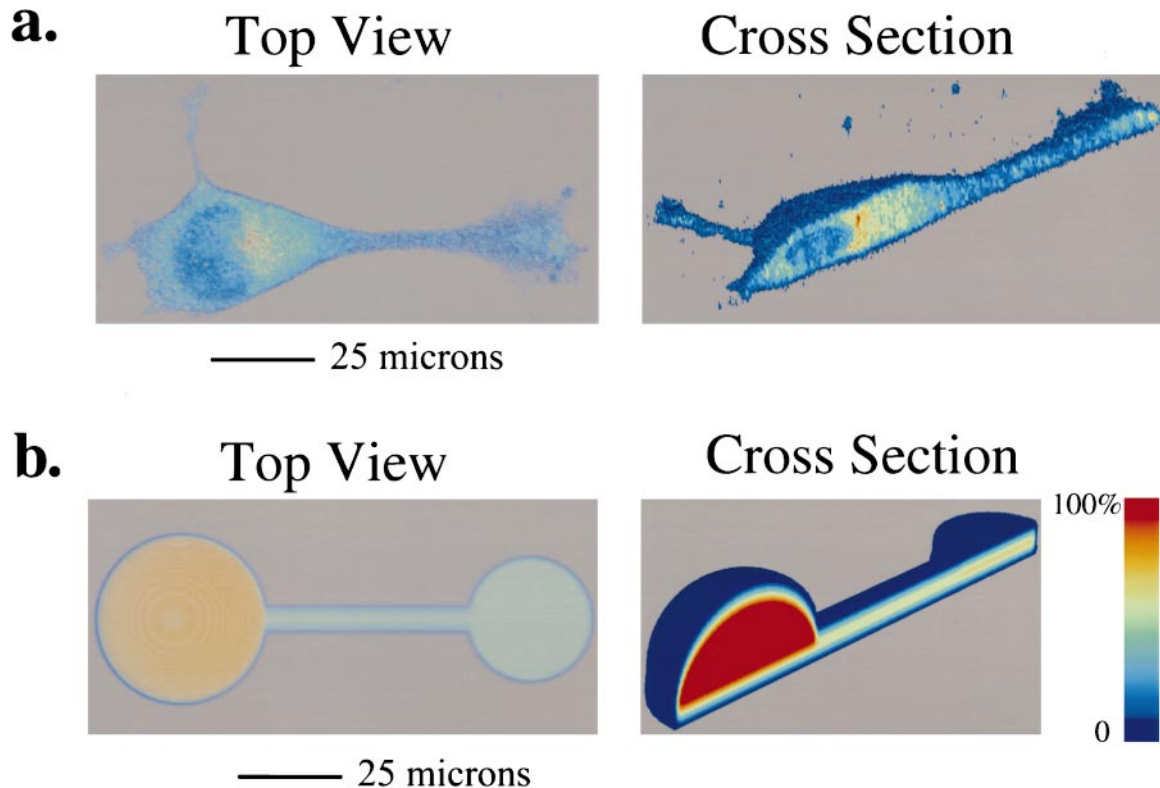

FIGURE 3 Distribution of a protein associated with the endoplasmic reticulum in a neuronal cell. (*a*) Volume rendering of a fixed neuroblastoma cell stained with anti-InsP$_3$ receptor. A *z*-series was taken with a 60×, NA 1.4 planapochromat oil immersion objective at 0.5-μm steps, and the resulting series was analyzed with VoxelView software. An overhead view of the cell is shown to the left, and a cross section through the central *xz* plane is shown to the right. (*b*) A model was constructed to represent the dimensions of the cell in *a*. The results of a convolution of the model with the PSF are shown here. The original full intensity is retained in the center of the soma of the blurred model, whereas the neurite intensity is reduced by $\sim$65%.

This idea is illustrated with the two models shown in Fig. 4 a. The models represent the essential geometric features of a neuronal cell plated on a coverslip: a large hemispherical soma, a thin semicylindrical neurite, and a small, flat growth cone. In both cases, the fluorescence from the subresolution membrane is significantly diluted by the convolution. The important issue, however, is whether the fluorescence remains proportionate in the three regions of the cell. For the model with the thick neurite (7 μm diameter), the peak membrane intensities in the neurite and the soma regions remain equal. For the thin neurite (3.5 μm), the blurred intensity associated with the soma is slightly higher (ratio of 0.85:1). This small loss of intensity in the smaller neurite can be attributed to its higher radius of curvature. Also

noteworthy is the intensity within the cell, attributable to blurred intensity from the flat membrane surface at the bottom of the model. When modeling cell membranes with this approach, it is important to create a model with sufficiently small voxels so that the entire surface can be represented as a single shell with no overlapping regions. For cells with very thin regions, such as the lamelipodia of fibroblasts, this will require very large models and correspondingly interpolated PSFs.

Our analysis may be applied to the distribution of bradykinin receptor in the N1E-115 neuroblastoma cells. These cells display calcium waves by an InsP$_3$-mediated pathway when exposed to bradykinin, and the wave invariably starts within the neurite (Fink et al., unpublished results). A pos-
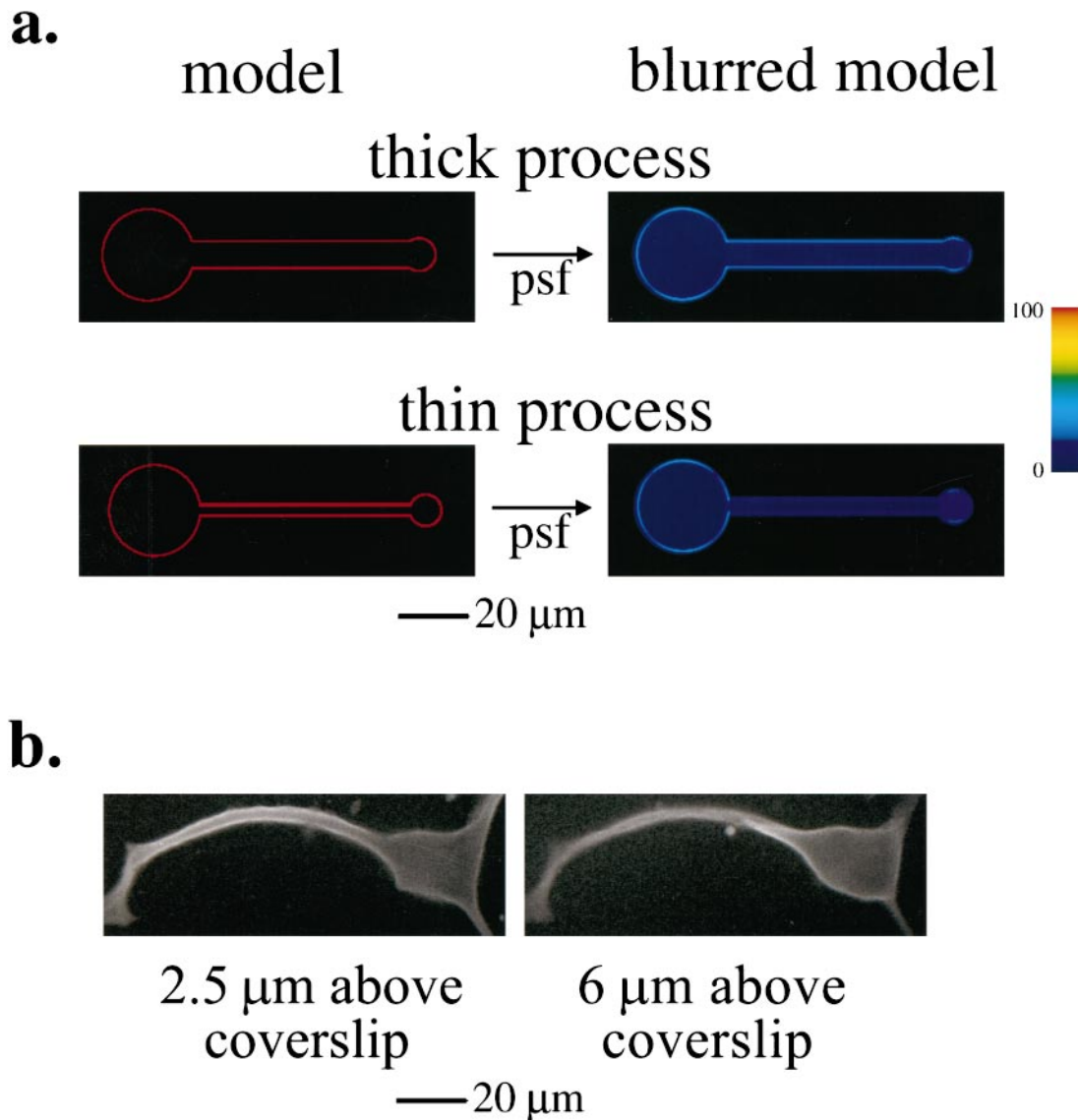

FIGURE 4 Pattern of fluorescence for a cell surface molecule in a neuronal cell. (a) Models of cells with thick and thin neurites are blurred with the PSF. Slices through the center of the neurite are shown in each case. The soma in each model is a hemispherical shell with a diameter of 25 μm; the neurites are semicylinders with diameters of 7 and 3.5 μm. (b) A fixed N1E-115 neuroblastoma was stained with rhodamine conjugated to an antibody against the B2 bradykinin receptor. A z-series was taken with a 60×, NA 1.4 objective at 0.5-μm steps on the confocal microscope. Slices from two planes are shown: one in which the process is in focus (close to the coverslip at 2.5 μm), and one in which the soma is in focus (further away from the coverslip at 6 μm).

sible explanation for the site of origin of the wave could be a higher density of bradykinin receptor in the neurite, leading to enhanced release of InsP$_3$ from this region of the cell membrane. Fig. 4 *b* shows two optical sections of a cell labeled with an antibody to the receptor. The upper model of Fig. 4 *a* was based on the general geometric features of this cell, and the PSF used to blur the model was obtained with the same optical configuration used for the images in Fig 4 *b*. The simplest interpretation of these images is that on average there is a larger density of bradykinin receptors on the surface of the neurite compared to the soma.

Membrane potential of individual mitochondria within a living cell

An appropriate Nernstian dye contains a delocalized positive charge and is sufficiently permeant that it can equilibrate rapidly through membranes. However, it should not be so hydrophobic that it binds significantly to the membrane. The ratio of fluorescence inside a compartment to that outside the compartment should be equal to the ratio of the respective dye concentrations, provided that each compartment is larger than the confocal depth of field. The ratio can then be plugged into the Nernst equation to calculate the potential across the membrane separating the compartments. The dyes TMRE and TMRM were introduced by this laboratory (Ehrenberg et al., 1988) for such measurements, and their application in confocal measurements of potential across the plasma membrane has been described (Farkas et al., 1989; Loew, 1993, 1998).

If the dimensions of a subresolution object filled with a fluorescent dye are known precisely, a blurred model can be generated to calibrate the dye intensity relative to that in a larger compartment with dimensions that encompass the confocal PSF. This is the idea behind our approach to measuring the relative concentrations of a Nernstian dye in the mitochondria and cytosol.

In an earlier study (Loew et al., 1993), it was shown that mitochondria in the neurites of the neuroblastoma cells are cylinders with remarkably uniform diameters of 230 nm. In the present work, we analyzed electron micrographs of mitochondria in NIH 3T3 fibroblasts (Fig. 5 *a*) and similarly found that they were twisted cylinders with diameters averaging 350 nm. The cylindrical axis was generally parallel to the plane of the substrate. Because the overall lengths of the cylinders were well above the *xy* resolution (~300 nm) of the microscope, a cylinder with a length of 1 μm and a diameter of 350 nm was chosen as an appropriate model for these mitochondria. A voxelized version of this cylinder at the resolution of the PSF is shown in Fig. 5 *b*, along with the results of the convolution. The original intensity of 10,000 units is substantially diluted, with a maximum intensity in the center of the blurred image of 1300 units; the ratio of the original intensity to the maximum of the blurred intensity provides the factor of 7.6 that is used to correct the mitochondrial intensity. In Fig. 6, this correction is applied to

one mitochondrion; the corrected intensity is divided by the intensity measured in an adjacent region of cytosol and plugged into the Nernst equation to determine the membrane potential. It is important to accurately determine the maximum intensity within the three-dimensional mitochondrion, so a number of planes must be sampled to be sure that the mitochondrion is correctly bracketed within the volume.

DISCUSSION

We have shown how confocal microscopy, when properly calibrated with PSF-convolved model images, can substitute for ratio imaging and double labeling to assess the distributions of intracellular structures and molecules. The analysis often clarifies interpretations that are not obvious by taking the image data at face value. A method is described to directly assay the intracellular concentration of a calcium indicator dye; this procedure may be applied to any fluorescent probe for which calibration solutions can be prepared. Another application was to the estimation of the pattern of distribution of both internal and plasma membrane-associated antigens. This can be especially valuable for studies of living cells where a reference colabel may be difficult to incorporate into an experiment. In particular, the distribution of specific proteins can be imaged by incorporating green fluorescent protein (GFP) or its mutants by molecular genetic techniques. Immunoflourescence colabeling is often precluded in these investigations because permeabilization and fixation are required to permit access of the reference antibody to the reference antigen. The approach described here can therefore be an especially valuable companion to GFP imaging of live cells when a realistic quantitative estimate of the GFP distribution is needed.

This work validates an assumption that was implicit in our use of Nernstian dyes to measure membrane potential in single cells (Farkas et al., 1989; Loew, 1993, 1998). The idea was that the confocal depth of focus is sufficiently narrow that it can be entirely encompassed within the thicker part of a cell (e.g., the nuclear region); therefore, the intensity measured from such a region can be directly related to concentration and compared to intensity measured in the extracellular space. The ratio of intensities from these two compartments should be equal to the ratio of concentrations of a permeant cationic dye like TMRE and can therefore be used directly to calculate the plasma membrane potential with the Nernst equation.

This work also represents an expansion of a concept that was originally used to correct residual blurring in restored (i.e., deconvolved) wide-field images of mitochondria (Loew et al., 1993). In that study, the 3D model mitochondrion was first blurred with the PSF of the wide-field microscope. The blurred model was then added back to a real 3D wide-field image so that it was artificially inserted into the center of the neurite of a differentiated neuroblastoma cell; this had the effect of introducing realistic noise characteristics to the model. This synthetic image was then

FIGURE 5 Model mitochondria from analysis of electron micrographs. (*a*) To develop a model for a mitochondrion based on accurate dimensions, we analyzed electron micrographs like the one illustrated here. Sections cut parallel to the substrate to encompass the thickness of the mitochondria were analyzed, and the mitochondria were found to be cylindrical, with varying lengths but relatively uniform diameters of 350 ± 65 (SD) nm. (*b*) The model, based on electron microscopy, is a cylinder with a length of 1000 nm and a diameter of 350 nm. It is sampled in a 3D grid consistent with the pixel resolution employed in the confocal microscope: 100 nm in *z* and 50 nm in *x* and *y*. The point spread function (PSF) is a 3D image of a 100-nm fluorescent bead added to the same coverslip holding the NIH 3T3 cells. The original intensity in the model is arbitrarily assigned to be 10,000 units. After convolution with the psf, the blurred model displays a maximum intensity of 1300 units. The ratio 10,000/1300 provides the calibration factor of 7.6 used in our modified Nernst equation.
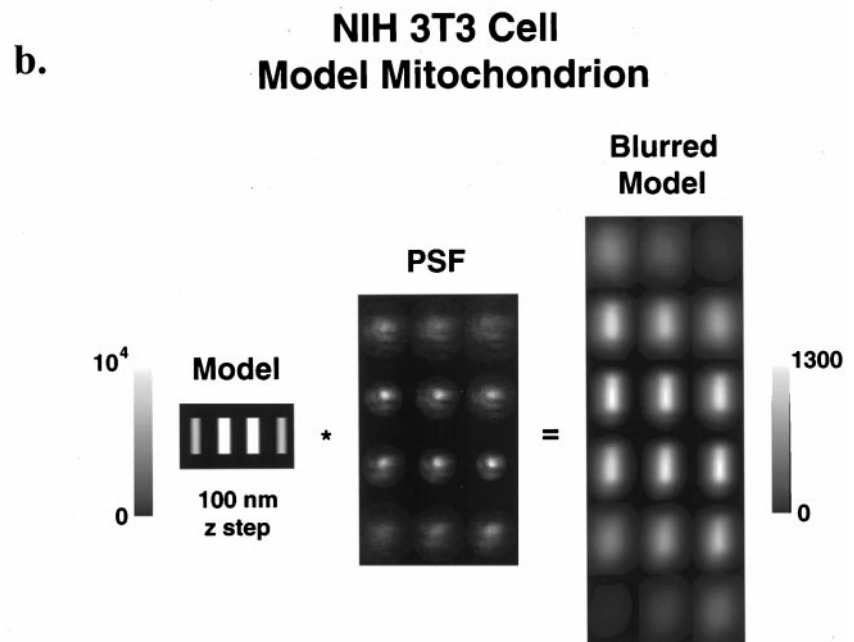
restored by deconvolution against the experimental PSF, and the resultant fluorescence intensity was related to the unblurred model to generate a calibration. The procedure developed here and based on confocal micrographs is considerably simpler. The correction factor of 7.6 in Fig. 5 was obtained with a pinhole setting that provided an acceptable fluorescence signal with a minimum of bleaching during acquisition of multiple optical sections. This is significantly higher than the values of 3–4 that were derived for the wide-field/restoration procedure. This is especially significant, given that the mitochondria in the NIH 3T3 cells are thicker (350 nm) than those in the neuroblastoma cell neurites (230 nm) used in our earlier study. Still, the mitochondrial membrane potentials that were derived from these measurements are realistic and close to those obtained in the

neuroblastoma cells. Indeed, the same procedures were applied to the neuroblastoma cells (data not shown) and provided mitochondrial membrane potentials that reproduced our earlier study, despite correction factors as high as 16. Therefore, even if correction factors are large, the corrections remain accurate.

On this basis, it might be expected that such corrections can be applied directly to wide-field images without the need to resort to deconvolution or confocal microscopy. For the mitochondria, correction factors on the order of 200 are necessary. Even if such large corrections could be tolerated, there are two other factors that mitigate against the use of wide-field images. First, the fluorescence of a given mitochondrion is not simply diluted by the cytosol and extracellular spaces, but may actually be enhanced by intensity

Membrane Potential of Mitochondria in NIH 3T3 Cell

0.3 μm steps

5 = F_cyt
155 = F_mit

$$V_{mit} = -60\log\left(\frac{7.6 * 155}{5}\right)$$

$$= -143\,mV$$

FIGURE 6 Determination of mitochondrial membrane potential in single mitochondria within live NIH 3T3 fibroblasts by confocal microscopy. A Zeiss LSM410 confocal microscope equipped with a 63× NA 1.4 planapochromat objective was used to measure TMRE fluorescence intensities from the cytosol (F_{cyt}) and the mitochondria (F_{mit}). Cells were treated with 100 nM dye and maintained on the stage at 37°. A cell is shown on the left, with the indicated rectangular region zoomed by a factor of 8 on the right. A set of five focal planes was acquired at 300-nm steps to ensure that the mitochondria to be analyzed were bracketed within the imaged volume. A membrane potential calculation for a typical mitochondrion is shown, using the calibration factor generated from the blurred model of Fig. 5 b.
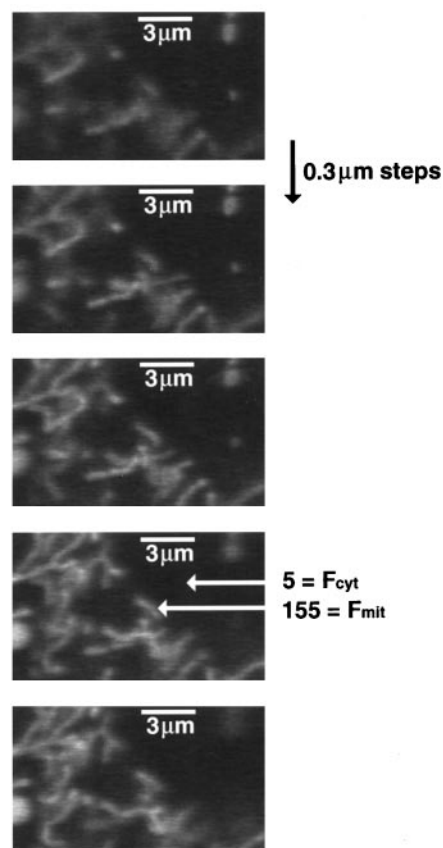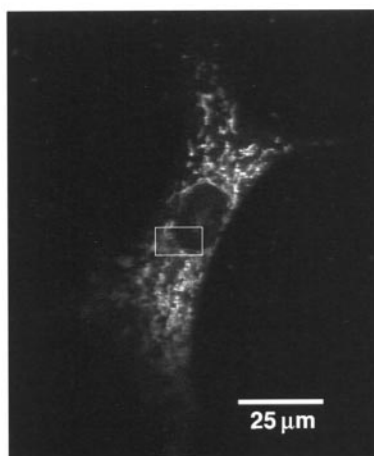
contributed by neighboring out-of-focus mitochondria. This effect, which is not addressed by the PSF convolution procedure, is largely absent in the high-resolution restored or confocal images. The second issue is that the cytosolic fluorescence, required for the denominator of the Nernst equation (Fig. 6), would be both hopelessly contaminated with out-of-focus mitochondrial fluorescence and diluted itself by the large wide-field PSF.

A more quantitative extension of the general technique could be realized by developing an algorithm for generating precise uniformly filled models based directly on experimental images of cells or subcellular organelles. This would make it possible to generate ratio images from an experimental image and the corresponding blurred model to quantitatively determine the spatial distribution of the fluorescent marker.

REFERENCES

Bright, G. R., G. W. Fisher, J. Rogowska, and D. L. Taylor. 1987. Fluorescence ratio imaging microscopy: temporal and spatial measurements of cytoplasmic pH. J. Cell Biol. 104:1019–1033.

Carrington, W. A. 1990. Image restoration in 3D microscopy with limited data. In Proceedings on Bioimaging and Two Dimensional Spectroscopy. L. C. Smith, editor. SPIE, Los Angeles. 72–83.

Carrington, W., and K. E. Fogarty. 1987. 3-D molecular distribution in living cells by deconvolution of optical sections using light microscopy. In Proceedings of the 13th annual Northeast Bioengineering Conference. K. Foster, editor. IEEE, New York. 108–111.

Carrington, W., K. E. Fogarty, and F. S. Fay. 1990. 3D fluorescence imaging of single cells using image restoration. In Non-invasive Techniques in Cell Biology. K. Foster, editor. Wiley-Liss, New York. 53–72.

Debiaso, R., G. R. Bright, L. A. Ernst, A. S. Waggoner, and D. L. Taylor. 1987. Five-parameter fluorescence imaging: wound healing of living Swiss 3T3 cells. J. Cell Biol. 105:1613–1622.

DeBiasio, R. L., L.-L. Wang, G. W. Fisher, and D. L. Taylor. 1988. The dynamic distribution of fluorescent analogues of actin and myosin in protrusions at the leading edge of migrating Swiss 3T3 fibroblasts. J. Cell Biol. 107:2631–2645.

Ehrenberg, B., V. Montana, M.-D. Wei, J. P. Wuskell, and L. M. Loew. 1988. Membrane potential can be determined in individual cells from the Nernstian distribution of cationic dyes. Biophys. J. 53:785–794.

Farkas, D. L., M. Wei, P. Febbroriello, J. H. Carson, and L. M. Loew. 1989. Simultaneous imaging of cell and mitochondrial membrane potential. Biophys. J. 56:1053–1069.

Fay, F. S., W. Carrington, and K. E. Fogarty. 1989. Threee-dimensional molecular distribution in single cells analyzed using the digital imaging microscope. J. Microsc. 153:133–149.

Grynkiewicz, G., M. Poenie, and R. Y. Tsien. 1985. A new generation of Ca^{2+} indicators with greatly improved fluorescence properties. J. Biol. Chem. 260:3440–3450.

Loew, L. M. 1993. Confocal microscopy of potentiometric fluorescent dyes. In Cell Biological Applications of Confocal Microscopy. Methods in Cell Biology, Vol. 38. B. Matsumoto, editor. Academic Press, Orlando. 194–209.

Loew, L. M. 1998. Measuring membrane potential in single cells with confocal microscopy. *In* Cell Biology: A Laboratory Handbook, Vol. 3. J. E. Celis, editor. Academic Press, San Diego. 375–379.

Loew, L. M., R. A. Tuft, W. Carrington, and F. S. Fay. 1993. Imaging in five dimensions: time dependent membrane potentials in individual mitochondria. *Biophys. J.* 65:2396–2407.

Tsien, R. Y., and M. Poenie. 1986. Fluorescence ratio imaging: a new window into intracellular ionic signaling. *Trends Biochem. Sci.* 11:450–455.

Wang, Y.-L., and D. L. Taylor. 1989a. Methods in Cell Biology, Vol. 29. Academic Press, San Diego.

Wang, Y.-L., and D. L. Taylor. 1989b. Methods in Cell Biology, Vol. 30. Academic Press, San Diego.